MFN= 007168
01 SID/SCD
02 5752
03 INPE-5752-PRE/1913
04 CEA
05 S
06 as
10 Clemesha, Barclay Robert
10 Simonich, Dale Martin
10 Takahashi, Hisao
10 Melo, H.
10 Plane, S.M.L.
12 Experimental evidence for photochemical control of the atmospheric sodium layer
14 18909-18916
30 Journal of Geophysical Research
31 100
32 D9
40 En
41 En
42 <E>
58 DAE
61 <PI>
64 Sept.<1995>
68 PRE
76 AERONOMIA
83 On May 31, 1992, a rocket payload equipped with 10 airglow photometers was launched from the Alcantara Launch Center in northern Brazil. The payload measured sodium, hydroxyl, atomic, and molecular oxygen airglow emissions, and a sodium lidar, operating at the launch site, provided simultaneous vertical profiles of atmospheric sodium density. The airglow profiles, in conjunction with the sodium density distribution, are used to derive vertical profiles for atomic oxygen, ozone and hydrogen in the 80 to 100 km region. These profiles are then used as inputs to a photochemical model for the sodium layer. Good agreement is achieved between the modeled and experimental profiles of sodium and Na D line airglow, and the results indicate that the branching ratio for the production of Na (2P) in the reaction NaO+O Na(2P, 2S)+O2 must be between 0.05 and 0.20.
90 B

JOURNAL OF GEOPHYSICAL RESEARCH, VOL. 100, NO. D9, PAGES 18,909-18,916, SEPTEMBER 20, 1995

Experimental evidence for photochemical control of the atmospheric sodium layer

B. R. Clemesha, D. M. Simonich, H. Takahashi and S. M. L. Melo
Instituto Nacional de Pesquisas Espaciais, São José dos Campos, São Paulo, Brazil

J. M. C. Plane
School of Environmental Sciences, University of East Anglia, Norwich, England

Abstract. On May 31, 1992, a rocket payload equipped with 10 airglow photometers was launched from the Alcântara Launch Center in northern Brazil. The payload measured sodium, hydroxyl, atomic, and molecular oxygen airglow emissions, and a sodium lidar, operating at the launch site, provided simultaneous vertical profiles of atmospheric sodium density. The airglow profiles, in conjunction with the sodium density distribution, are used to derive vertical profiles for atomic oxygen, ozone and hydrogen in the 80 to 100 km region. These profiles are then used as inputs to a photochemical model for the sodium layer. Good agreement is achieved between the modeled and experimental profiles of sodium and Na D line airglow, and the results indicate that the branching ratio for the production of $Na(^2P)$ in the reaction $NaO + O \rightarrow Na(^2P, ^2S) + O_2$ must be between 0.05 and 0.20.

Introduction

Although there is little doubt that the source of the atmospheric sodium layer is the meteor deposition of extraterrestrial material, the processes which lead to the formation of a sharply bounded layer, between 80 and 110 km, are still open to discussion. The rapidly increasing mixing ratio of atomic oxygen above about 90 km makes the atmosphere strongly reducing in this region, so it would be expected that metallic compounds should be reduced to free metals. In the absence of other processes this would cause the sodium mixing ratio to be constant above the meteor ablation source region. In fact, the scale height of the sodium layer at heights above 100 km is about half that of the main atmospheric constituents, and it is generally assumed that ionization provides the necessary loss mechanism. With respect to the bottomside of the layer, a number of possible loss mechanisms for the removal of sodium have been suggested in the literature: these include oxidation, mainly by O_2 and O_3, the formation of cluster ions, and attachment to aerosol particles. Oxidation/reduction schemes have been discussed by many workers including, for example, *Hunten* [1967], *Megie and Blamont* [1977], *Kirchhoff et al.* [1981], *Sze et al.* [1982], *Swider* [1986], and *Plane* [1991]. The possible importance of cluster ions was first suggested *by Richter and Sechrist* [1979], and investigated in greater detail by *Jegou et al.* [1985a, b] and *Granier et al.* [1985]. *Hunten* [1981] suggested that meteor ablation, generally accepted as the source of atmospheric sodium, also results in the formation of micron size "smoke" particles which act as a sink for free sodium atoms. Each of the mechanisms investigated has been shown to be capable of adequately simulating the vertical distribution of atmospheric sodium. Although photochemical schemes have received considerably more attention than the other two, there are no very convincing reasons to reject the latter, and adequate experimental evidence required for the evaluation of photochemical models is lacking. We have many accurate measurements of the vertical profile of free sodium, but no simultaneous direct measurements of the other atmospheric constituents which might be involved. The purpose of this paper is to present the results of an experiment in which the vertical distribution of free sodium was measured by lidar at the same time as a rocket payload measured airglow emissions from atomic and molecular oxygen, hydroxyl and sodium. Since these emissions are related to the vertical profiles of atomic oxygen, ozone and hydrogen, the experiment enables us to evaluate the predictions of a photochemical model for the atmospheric sodium layer.

Copyright 1995 by the American Geophysical Union.

Paper number 95JD01708.
0148-0227/95/95JD-01708$05.00

Measurements

Figure 1 shows a simplified diagram of the MULTIFOT payload, launched from the Alcântara Launch Center (2°S, 44°W) on a SONDA III rocket at 2352 LST on May 31, 1992. The payload contained 6 forward looking (longitudinal) and 4 side looking (transverse) photometers. The longitudinal photometers were protected by a conventional split nose cone during launch, and the four transverse photometers, situated below the longitudinal instruments, viewed the atmosphere at right angles to the rocket axis through 5-cm quartz windows inserted into the payload skin. Launch parameters are given in Table 1, and specifications for the photometers are shown in Table 2. In an earlier paper [*Clemesha et al.*, 1993] we presented the measured profile for the Na D emission. Together with the vertical distribution of free sodium, measured by lidar, the Na D profile was used to determine mesospheric ozone. In the present report we shall use the profiles for the atomic and molecular oxygen emissions, together with the OH and sodium emissions, to estimate the vertical profiles of

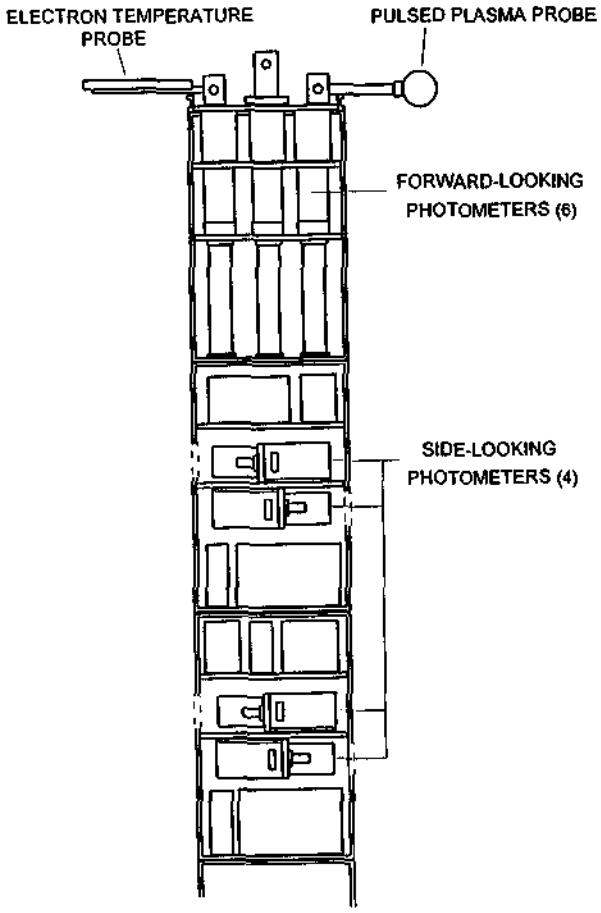

Figure 1. MULTIFOT airglow payload.

O, O_3, and H to be used in a complete photochemical model of the atmospheric sodium layer.

The payload was designed to study the vertical emission profiles of the O_2 Herzberg, OI 557.7 nm, Na D, OI 630 nm, OH(8,3) and O_2 Atmospheric (0,0) band emissions. The photon-counting photometers were similar in principle to those described *by Takahashi et al.* [1987]. Data were telemetered at 250 10-bit samples per second for each instrument. A 2-axis magnetometer was used for attitude determination. Absolute laboratory calibrations of all photometers were carried out prior to launch, as described by *Takahashi et al.* [1987], and each instrument included an in-flight calibration source.

A longitudinal photometer for 578 nm and a transverse instrument for 713 nm were included to estimate the background continuum. Unfortunately, the 713-nm transverse photometer failed shortly after launch, making it difficult to estimate the background for the transverse photometers. This created a serious problem with respect to the analysis of the Na D emission profile, where the background should contribute a significant fraction of the total detected signal. For this reason we used the data from the longitudinal 589.3-nm photometer to determine the Na D profile. In any case, the closer proximity in wavelength of the 578-nm photometer makes the background subtraction more reliable. For the much stronger OH emission the lack of an accurate background signal is much less important.

Table 1. Launch Parameters

Parameter	Value
Vehicle	SONDA III
Date	31/05/92
Time	2352 LST
Location	Alcântara Launch Center (2°S, 44°W)
Apogee	282 km
Ground range	398 km

Measurements of the vertical profile of atmospheric sodium density were made using the transportable lidar system illustrated in Figure 2, specifications of which are given in Table 3. The lidar included a sodium vapor cell for calibration purposes, and is similar in principle (although not in its mechanical layout) to the São José lidar described by *Simonich et al.* [1979] and *Clemesha* [1984]. The equipment was installed at the launch site, about 5 km from the ramp, and was operated throughout the campaign. Sky conditions were unfavorable during most of the campaign, and most lidar data were obtained by firing through gaps in the cloud cover. For this reason the signal to noise ratio of the profiles obtained was poor when compared with typical results from modern lidars. On the other hand, on the night of the rocket experiment, adequate profiles were obtained both before and during the launch.

Emission rate profiles were derived from both the transverse and longitudinal photometers. The technique used for deriving the vertical profile of volume emission rate from the longitudinal photometer signal was identical to that described by *Takahashi et al.* [1987], using the incremental straight-line fitting technique of *Murtagh et al.* [1984], with a 4-km fitting length. To determine the OH(8,3) band intensity from the 724.2-nm side looking photometer signals we applied a suitable inversion process to the observed horizon intensity profile (horizon intensity, in this context, refers to the intensity seen by the photometer when its viewing angle is horizontal). The 2° field of view of the photometer was taken into account by deconvolving the inverted profile with an appropriate instrument function. In the present study, profiles from the longitudinal photometers were used for Na D and the O_2 Atmospheric band, and the profile from the 724.2-nm side looking photometer was used for the OH(8,3) band profile.

Table 2. MULTIFOT Photometer Specifications

Wavelength, nm	Bandwidth, nm	PMT	Sensitivity*
	Side looking photometers		
589.3	1.75	EMI 9924	84.1
630.0	1.57	EMI 9798	21.6
713.0	10.90	EMI 9798	...
724.2	1.75	EMI 9798	41.4
	Forward looking photometers		
275.0	14.30	EMI 9924	267.6
557.7	1.66	EMI 9924	684.0
578.0	10.95	EMI 9924	165.4
589.3	1.69	EMI 9924	326.9
724.2	1.91	EMI 9798	143.9
762.0	5.69	EMI 9798	43.6

* Measured in counts sec^{-1} $Rayleighs^{-1}$

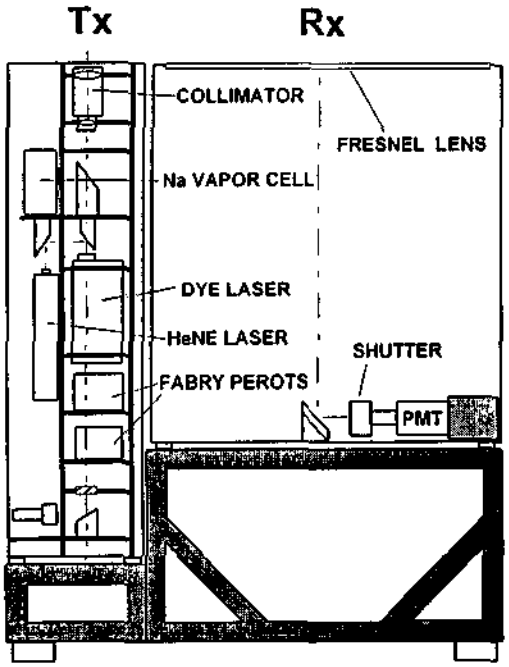

Figure 2. Transportable lidar.

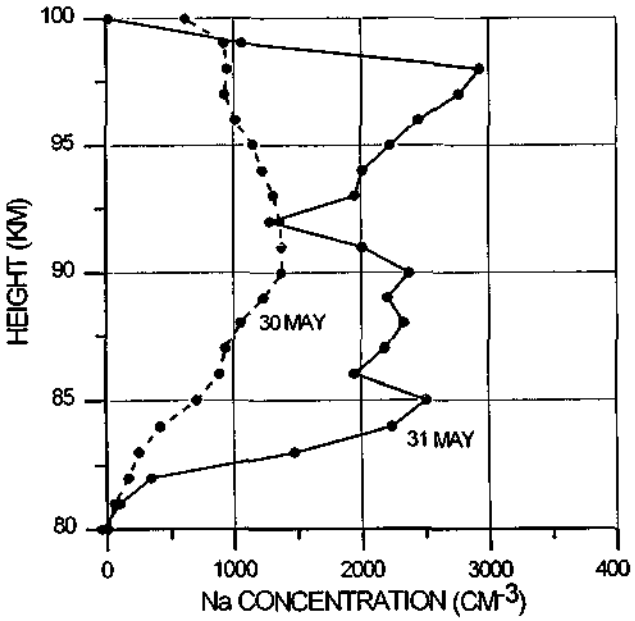

Figure 3. Lidar profiles of Na density.

Further details of the rocket experiment and the associated data analysis will be presented elsewhere.

The upleg trajectory of the SONDA III rocket was such that it passed through the sodium layer at a distance of about 40 km downrange from the lidar. In view of this horizontal displacement between the lidar measurement and the rocket, together with the poor signal to noise ratio for the lidar, it was considered best to average the lidar data over a 1-hour period centered on the launch time. The resulting profile, labeled 31 May, is shown in Figure 3. This profile shows an unusually steep gradient in sodium density between the heights of 82 and 84 km. The average profile for the previous night, also shown in Figure 3, and labeled 30 May, shows a much more typical height distribution, with an approximately linear increase between 80 and 90 km.

The airglow profiles used are shown in Figure 4. The profile for the sodium emission shown in Figure 4 was derived from the upleg data, so as to minimize the horizontal distance between the lidar measurement of the sodium concentration and the rocket observation of the sodium emission profile. This is important because the ozone concentration is obtained from the ratio between the Na D intensity and the sodium density. Because of the steep vertical gradients in sodium density and airglow intensity a fairly small vertical displacement of the layer could result in large errors in the ozone concentration. Downleg data were used for the other emissions because contamination effects obliterated the signals from the longitudinal infrared photometers during the upleg. The downleg passage through the emitting region occurred approximately 370 km downrange from the launch ramp. The upleg and downleg OH(8,3) emission profiles derived from the 724.2 nm transverse photometer were found to be very similar, so on this basis we should not expect the horizontal separation between the locations corresponding to the lidar measurement and the airglow profiles to seriously affect the comparison. On the other hand, the downleg profile for OH derived from the longitudinal photometer shows emission intensities almost twice those determined from the transverse photometer. The transverse photometers view a

Table 3. PORTAL Lidar Specifications

Dye laser transmitter	Receiver
Wavelength, 589 nm	Fresnel lens, 0.4 m^2
Bandwidth, 6 pm	bandwidth, 1 nm
Pulse length, 2 μs	height resolution, 250 m
Repetition rate, 1 pps	efficiency, 1 %

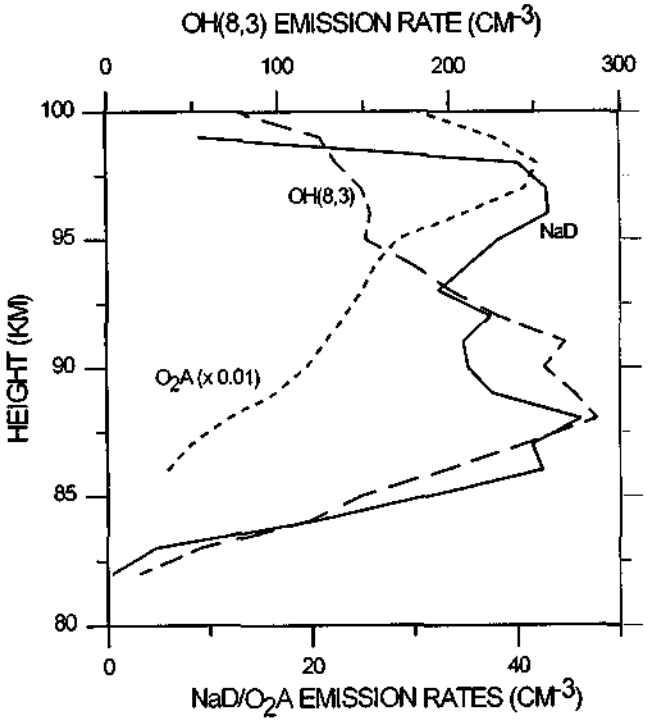

Figure 4. Volume emission rate profiles.

horizontal section through the emission layer several hundred km in extent, whereas the longitudinal photometers make an almost local measurement. It seems likely that the high intensity seen by the longitudinal OH photometer corresponded to a region of enhanced emission at the location of the downleg passage through the emission layer. This conclusion in supported by the fact that an analysis of the signals from the transverse photometer when the payload was above the layer, where the payload rotation causes the photometer to scan the emitting layer, shows the existence of considerable small-scale structure.

From Figures 3 and 4 it can be seen that below 90 km there is a remarkable degree of similarity between the emission profiles for the OH(8,3) band and the Na D line emission, and that the NaD profile is very similar to the vertical distribution of free sodium. In the next section we show that this similarity is consistent with a photochemical model for the atmospheric sodium layer.

Model Calculations

The model of sodium in the upper atmosphere that is employed here has been described in detail by *Helmer and Plane* [1993]. This model assumes that (1) the source of mesospheric sodium is meteoric ablation; (2) sodium is partitioned through 26 reactions among nine constituent gas-phase species (Na, Na^+, Na cluster ions, NaO, NaO_2, NaO_3, NaOH, $NaCO_3$ and $NaHCO_3$); (3) the partitioning is rapid on the time-scale of vertical mixing between 80 and 100 km; and (4), heterogeneous reactions on meteoric dust particles are of limited importance. Since the transport of all sodium constituents is then governed by the same eddy diffusion coefficient, the continuity equation for total sodium (Na_{tot}) can be solved [*Plane*, 1991]. The solution requires knowledge of the injection rate of Na as a function of altitude, which may be determined from the total meteoric ablation flux of Na (estimated by *Junge et al.* [1962] to be 1.3×10^4 atoms cm^{-2} s^{-1}) together with the meteoric ablation profile [*Hunten et al.*, 1980]. It is also necessary to specify the Na_{tot} density at 65 km, the lower boundary of the model. In this work we have used the value of 7×10^4 molecule cm^{-3}, adopted by *Helmer and Plane* [1993]. This value was chosen to make the model generate the column density of atomic Na observed during winter at 69°N, where the sodium layer has been studied over a number of years and is comparatively stable [*Tilgner and von Zahn*, 1988].

For the present study, the temperature profile was derived using the MSIS model [*Hedin*, 1987] above 90 km, and the CIRA 86 temperature profile (for May at the equator) at lower heights [*Fleming et al.*, 1990], with a small adjustment to make the temperature profile agree with a ground-based measurement of the OH rotational temperature at the time of the launch. The atmospheric density was then computed for hydrostatic equilibrium, with the mixing ratios of N_2 and O_2 from the MSIS model. A brief description of how the vertical distributions of O, O_3, and H were derived from the airglow profiles is given in the following paragraphs; a more complete description is being presented elsewhere (H. Takahashi et al., Atomic hydrogen and ozone concentrations derived from simultaneous lidar and rocket airglow measurements in the equatorial region, submitted to Journal of Geophysical Research, 1994).

The atomic oxygen concentration (shown in Figure 5) was derived from the OH(8,3) emission measured by the transverse photometer from 82 to 85 km, and from the O_2 (0,0) emission above this height. The O_2 emission was used because it is much stronger than the $O(^1S)$, so that the errors in deriving the emission profile from the integrated intensity seen by the photometer are much smaller. The Barth mechanism is now generally accepted for the production of $O_2(b^1\Sigma_g^+)$, responsible for the O_2 emission via a precursor state, as yet unidentified [*McDade et al.*, 1986]. As a result of this, the appropriate transition probabilities required to relate the emission intensity to the atomic oxygen concentration are not known. In this study we used empirical parameters derived by *McDade et al.* [1986], from a rocket experiment in which the O_2 (0,0) and OI 557.7 nm emission rates were measured simultaneously with the atomic oxygen concentration. Since McDade's parameters have been confirmed by subsequent studies by *Murtagh et al.* [1990] and *López-Gonzalez et al.* [1992], we adopt them with some degree of confidence.

To determine the atomic oxygen concentration from the OH(8,3) intensity it was assumed that excited OH is produced in the catalytic destruction of ozone by the reaction $H + O_3 \rightarrow OH^* + O_2$, and that this reaction is in quasi-equilibrium with $O + O_2 + M \rightarrow O_3 + M$. In our analysis we used the parameters presented by *McDade et al.* [1987] for single-step collisional cascade type quenching. The transition probabilities used by *McDade et al.* [1987] are those of *Murphy* [1971].

As in the paper by *Clemesha et al.* [1993], the vertical ozone profile was derived from the measured sodium density and airglow intensity profiles, illustrated in Figures 3 and 4, by assuming that the Na D-line airglow is produced by the Chapman mechanism:

$$Na + O_3 \rightarrow NaO + O_2 \quad (1)$$

$$NaO + O \rightarrow Na(^2P, ^2S) + O_2 \quad (2)$$

Na and NaO should exist in a kinetic steady state since both reactions 1 and 2 are rapid [*Plane*, 1991]. Hence the

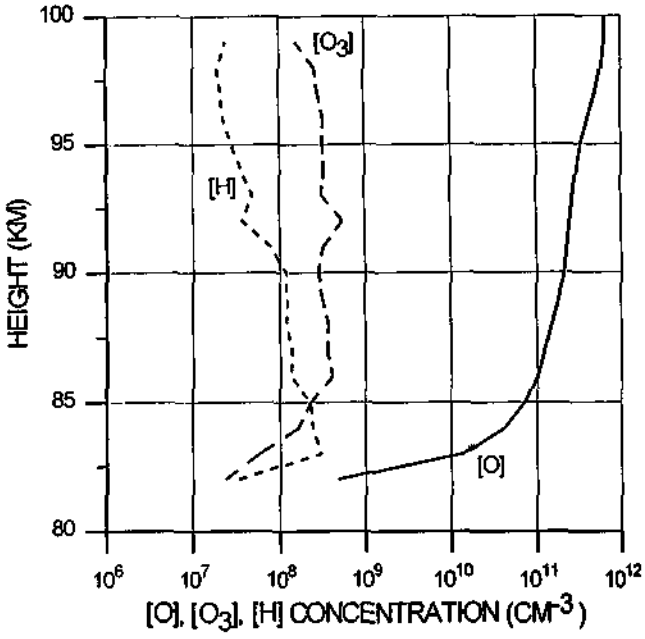

Figure 5. Derived profiles of O, O_3, and H.

NaD emission rate is equal to $k_1\alpha$[Na] [O3], where α is the branching ratio of (2) that produces Na(^{2}P). The value of k_1 has been measured recently at mesospheric temperatures [*Plane et al.*, 1993], so that the ozone concentration can be retrieved if α is known. The atomic hydrogen profile can then be derived from the atomic oxygen and ozone profiles, again assuming a steady-state between the termolecular production of ozone and its destruction by the H + O_3 reaction. In the present study the rate coefficients for these reactions were taken from *DeMore et al.* [1990].

Unfortunately, α is very difficult to measure experimentally and the Chapman scheme is further complicated because both (1) and (2) involve the excited $^2\Sigma^+$ electronic state of NaO (see below). Thus we decided to run the sodium model of *Helmer and Plane* [1993] with α as the only adjustable parameter. The value of α was varied until the modeled column abundance of atomic Na below 90 km was equal to that measured by the lidar (Figure 3). The upper limit of 90 km was chosen because the Na layer is controlled by ionic rather than neutral chemistry above this height [*Plane*, 1991]. This fitting procedure yielded a value for α of 0.093, very close to the value of 0.1 which *Helmer and Plane* [1993] found necessary to generate a modeled nightglow intensity in accord with observations at high latitudes. The resulting profiles of ozone and hydrogen are illustrated in Figure 5. The O_3 densities between 80 and 90 km are factors of 3 to 6 higher than the average daytime concentrations during May measured by the Solar Mesospheric Explorer (SME) satellite which monitors the 1.27-μm airglow [*Keating et al.*, 1990]. However, a nighttime increase in O_3 of this magnitude is expected from other observations and theoretical models [e.g., *Allen et al.*, 1984; *Solomon et al.*, 1986]. The atomic hydrogen densities are in sensible accord with direct rocket-borne measurements of this species [e.g., *Sharp and Kita*, 1987]. It should be noted that the ozone concentrations shown in Figure 5 are much larger than those presented by *Clemesha et al.* [1993] because a value of 0.67 was used for α in the earlier publication.

Discussion and Conclusions

Figure 6 illustrates a comparison between the atomic Na profile observed by lidar, and the model profile calculated with α = 0.093. Figure 7 shows a comparison between the observed and modeled NaD airglow intensity profiles. In both cases it will be seen that rather good agreement is achieved between model and observation, particularly in reproducing the unusually small scale-heights on the undersides of the atomic Na and airglow layers, where there is a steep cutoff between 84 and 82 km. The significant discrepancies between model and observation that appear above 87 km are probably caused by several factors. First, the model generates a time-averaged profile of the Na_{tot} density, derived from the meteoric source function and the eddy diffusion coefficient. This profile is illustrated in Figure 8, along with the profile of Na_{tot} density that would exactly reproduce the lidar observations of atomic Na. The oscillations of the second profile about the average profile are most likely short-term fluctuations caused by the action of gravity waves and tidal forcing [*Batista et al.*, 1985; *Gardner and Voelz*, 1987], and by the sporadic nature of the Na injection from meteoric ablation. Another factor leading to the poor agreement between model and observation above 94 km is that without in

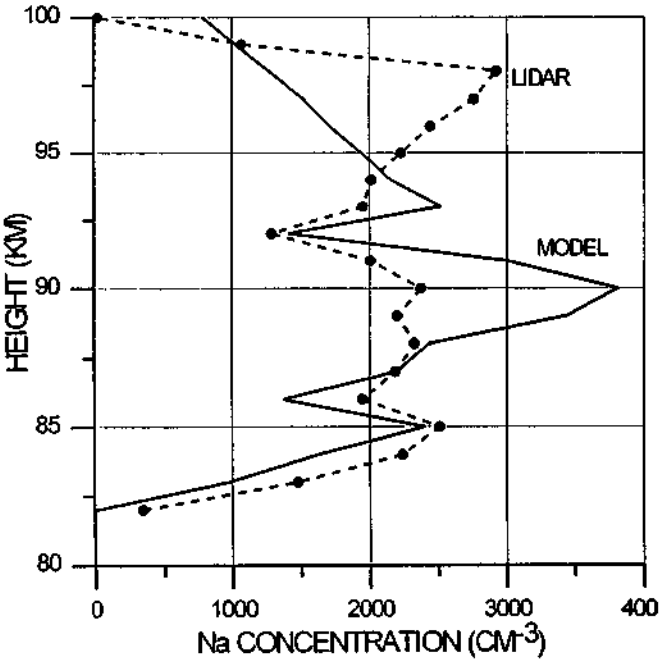

Figure 6. Comparison between observed and modeled profiles of atomic Na concentration.

situ measurements of the relevant ionic species during the rocket flight, typical concentrations of the major ions NO^+ and O_2^+ and the electron density [*Thomas et al.*, 1983] have had to be assumed in the model. In fact, the secondary peak of atomic Na observed at 97 km (Figure 6) could possibly be a small sporadic sodium layer [e.g. *Batista et al.*, 1989], which may be caused by the layering and neutralization of Na^+ ions [*Cox et al.*, 1993]. As would therefore be expected, the more "typical" Na layer observed on 30 May, 1992 (Figure 3) is in better accord with the model, peaking at 90 km and displaying a gradual decrease at higher altitudes.

Figure 9 illustrates the modeled profiles of the major Na constituents. $NaHCO_3$ is the major sink for Na below 88 km because the reaction

$$NaHCO_3 + H \rightarrow Na + H_2CO_3 \quad (3)$$

is the only likely removal process for $NaHCO_3$ in the mesosphere [*Rajasekhar and Plane*, 1993] and k_3 is small [*Ager and Howard*, 1987]. NaO_2 is a much less important reservoir for Na because the reaction

$$NaO_2 + O \rightarrow NaO + O_2 \quad (4)$$

is fast enough to ensure that the lifetime of NaO_2 is short above 80 km [*Helmer and Plane*, 1993]. This is a change from earlier photochemical models [e.g., *Sze et al.*, 1982; *Thomas et al.*, 1983; *Kirchhoff*, 1983; *Swider*, 1986] which predicted that NaO_2 (or NaOH, below 80 km, in the case of *Swider's* [1986] model) would be the major form of Na below 85 km. Although the possibility that $NaHCO_3$ might be involved in the Na chemistry had already been suggested by *Murad and Swider* [1979], these models did not have available the recently measured rate coefficient for (4) [*Ager and Howard*, 1987], and did not include the chemistry of $NaHCO_3$ [*Helmer and Plane*, 1994].

Thus, the rapid decrease in the atomic Na concentration on the underside of the layer is mainly caused by the corresponding decrease in atomic H and O (see Figure 5). It should be

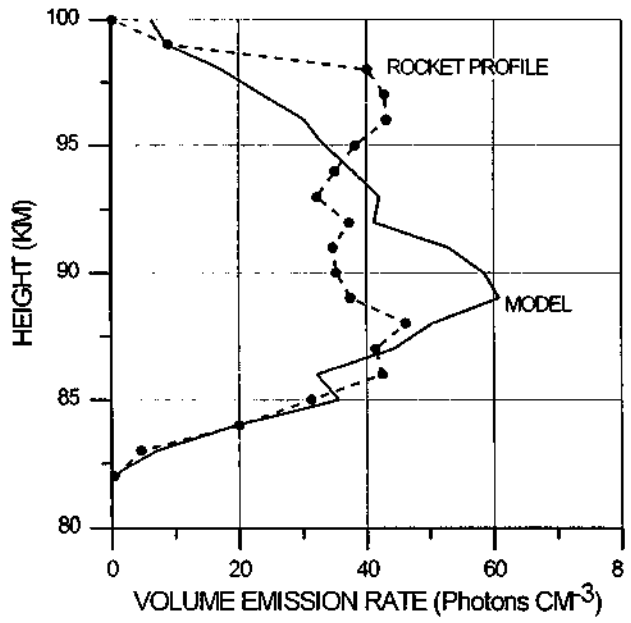

Figure 7. Comparison between observed and modeled profiles of the Na D-line airglow emission intensity.

noted that neither the cluster-ion model of *Jegou et al.* [1985a] nor the aerosol attachment mechanism proposed by *Hunten* [1981] would respond to the sharp gradients in atomic H and O in this way.

Finally, the simultaneous observations of the atomic Na and the NaD emission profiles have enabled us to conclude that α is about 0.1. This value, based as it is on a comprehensive model using input data from a simultaneous measurement of the sodium concentration and airglow profiles, should be considerably more reliable than earlier estimates.

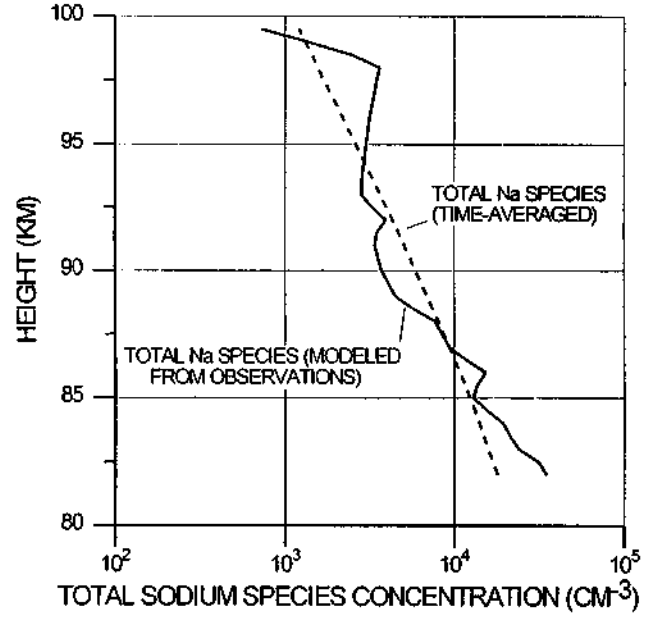

Figure 8. Vertical profile of the total concentration of Na-containing species calculated using a time-averaged Na injection rate from meteor ablation, compared with a profile that would give exact agreement between the model and lidar observations.

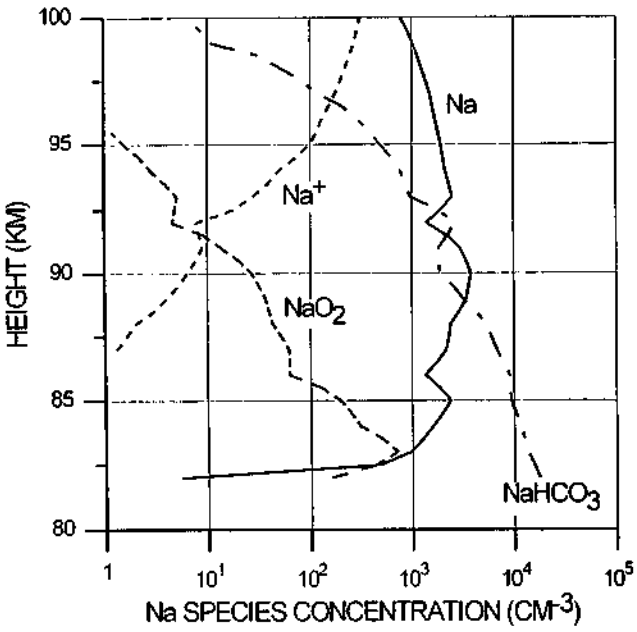

Figure 9. Vertical profiles of the major sodium species.

The value of 1/3 for α estimated by *Bates and Ohja* [1980] was based on typical integrated NaD intensities, Na abundances and ozone concentrations, rather than actual simultaneous measurements. *Swider* [1980] also used 1/3, apparently on the basis of simultaneous measurements of the sodium profile and the integrated airglow intensity measured by a ground-based photometer, published by *Clemesha et al.* [1978]. There appears to have been only one reported laboratory measurement of this branching ratio. *Plane and Husain* [1986] obtained an upper limit to α of 0.01, which is therefore smaller by about an order of magnitude than the values required in the model to match the airglow intensity. How-

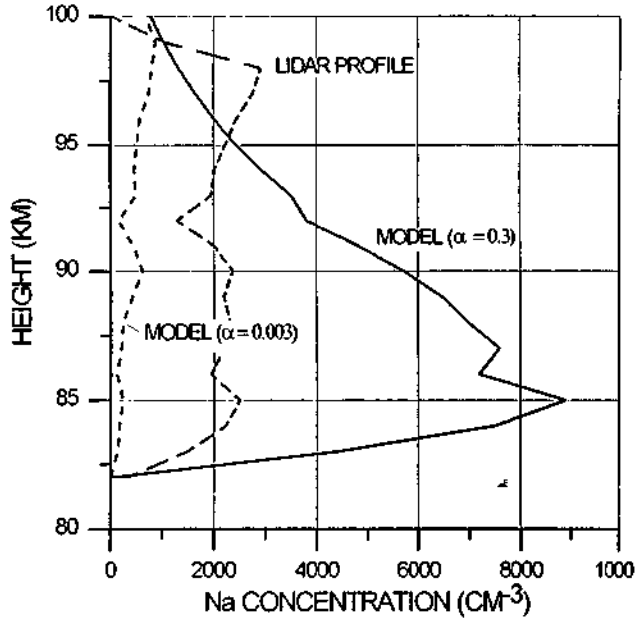

Figure 10. A comparison between the observed atomic Na density profile and profiles calculated from the model using upper and lower limits to the branching ratio α.

ever, recent work by *Wright et al.* [1993] and *Shi et al.* [1993] has shown that reaction 1 produces NaO almost entirely in the first excited $^2\Sigma^+$ state, rather than the ground $^2\Pi$ state. *Herschbach et al.* [1992] have used electronic symmetry correlation to show that the reaction $NaO(^2\Sigma^+) + O \rightarrow Na(^2P) + O_2$ could have a branching ratio α ranging from 0.5 to 0.67. Thus, if the removal of $NaO(^2\Sigma^+)$ by spontaneous emission or by quenching with N_2 or O_2 is slow compared to reaction with atomic O between 80 and 90 km, this would account for the observed airglow intensities. It would also reconcile the low experimental estimate of α by *Plane and Husain* [1986], since their experiment most probably observed the reaction of atomic O with ground-state $NaO(^2\Pi)$ only. However, the precise role of $NaO(^2\Sigma^+)$ in the airglow emission remains to be quantified through future laboratory investigations.

In this study we have assumed that α is an overall branching ratio describing the production of $Na(^2P)$ from the reaction of both states of NaO with O, and that the physical quenching of $NaO(^2\Sigma^+)$ does not significantly affect α so that this branching ratio is constant with height. We can now use the present set of observations to determine the probable range of α about the best fit value of 0.1. Figure 10 shows the modeled atomic Na profiles that are obtained when α is increased or decreased by a factor of 3. It will be seen that changing α has a significant effect both on the atomic Na column density and on the peak height of the layer. For instance, when α is set to 0.3, the calculated O_3 concentration in the model is reduced because less O_3 is required to generate the observed D line airglow intensity. This in turn increases the atomic H concentration, since this is derived from the O_3 and atomic O densities (see earlier). Thus the rate of oxidation of atomic Na by (1) is slower, while the rate of reduction of $NaHCO_3$ by (3) is faster. This leads to a more than threefold increase in the column density of atomic Na, and a lowering of the peak of the layer to 85 km.

In fact, the modeled column density is not a particularly sensitive test of the choice of α because the column density of atomic Na is governed by the profile of Na_{tot}, which is a function of the Na injection rate from meteoric ablation and the eddy diffusion coefficient. There is considerable uncertainty about the injection rate [e.g. *Cox et al.*, 1993], and the eddy diffusion coefficient profile could certainly vary by a factor of 3 about the global mean value employed in the present model [*Hocking*, 1990]. Thus the modeled Na column density can be reconciled with the observed value if the Na injection rate is reduced by a factor of between 2 and 4, and the eddy diffusion coefficient is increased by a similar factor. However, the layer still peaks at 85 km, which is about 5 km too low, and the O_3 densities determined with $\alpha = 0.3$ are smaller by about a factor of 2 than predicted from the SME daytime average values [*Keating et al.*, 1990].

When α is set to 0.03, the column density is decreased by more than a factor of 3 and the peak height is raised to 99 km (Figure 10). Although the column density can be reconciled with the lidar measurement by decreasing the eddy diffusion coefficient by a factor of 3 and increasing the Na injection rate by a similar factor, the layer peak at 99 km is about 9 km too high, and the O_3 densities are about a factor of 4 higher than expected from the SME daytime average. Thus, the best-fit value for α of about 0.1 appears to be reliable within a factor of 2.

In conclusion, the modeling of this unique set of observations has provided strong evidence that the chemistry of the Na layer below 90 km can be adequately described by competition between the oxidation of atomic Na by O_3 and O_2, and the reduction of $NaHCO_3$ and NaO_2 by atomic H and O. In addition, our analysis indicates that the overall branching ratio for the production of $Na(^2P)$ via the Chapman mechanism most probably lies in the range 0.05 - 0.2.

Acknowledgments. We are grateful to the many people who made the rocket experiment possible. Special thanks are due to Agnaldo Eras and Narli Baesso, who designed and built most of the payload, to the IAE team responsible for the SONDA III vehicle, and to the personnel of the Alcântara Launch Center. This work was carried out in cooperation with the Instituto de Aeronáutica e Espaço - IAE.

References

Ager, J. W., and C. J. Howard, Rate coefficient for the gas phase reaction of NaOH with CO_2, *J. Geophys. Res., 92*, 6675- 6678, 1987.

Allen, M., J. I. Lunine, and Y. L. Yung, The vertical distribution of ozone in the mesosphere and lower thermosphere, *J. Geophys. Res., 89*, 4841-4872, 1984.

Bates, D. R., and P. C. Ohja, Excitation of the Na D-doublet of the nightglow, *Nature, 286*, 790-791, 1980.

Batista, P. P., B. R. Clemesha, D. M. Simonich, and V. W. J. H. Kirchhoff, Tidal oscillations in the atmospheric sodium layer, *J. Geophys. Res., 90*, 3881-3888, 1985.

Batista, P. P, B. R. Clemesha, I. S. Batista, and D. M Simonich, Characteristics of the sporadic sodium layers observed at 23° S, *J. Geophys. Res., 94*, 15349-15358, 1989.

Chapman, S., Notes on atmospheric sodium, *Astrophys. J., 90*, 309-316, 1939.

Clemesha, B. R., Lidar studies of the alkali metals, *Middle Atmos. Handb., 13*, 99-112, 1984.

Clemesha, B. R., V. W. J. H. Kirchhoff, and D. M. Simonich, Simultaneous observations of the Na 5893 A nightglow and the distribution of Na atoms in the mesosphere, *J. Geophys. Res., 83*, 2499-2503, 1978.

Clemesha, B. R., D. M. Simonich, H. Takahashi, and S. M. L. Melo, A simultaneous measurement of the vertical profiles of sodium nightglow and atomic sodium density in the upper atmosphere, *Geophys. Res. Lett., 20*, 1347-1350, 1993.

Cox, R. M., J. M. C. Plane, and J. S. A. Green, A modeling investigation of sudden sodium layers, *Geophys. Res. Lett., 20*, 2841-2844, 1993.

DeMore, W. B., S. P. Sander, D. M. Golden, M. J. Molina, R. F. Hampson, M. J. Kurylo, C. J. Howard, and A. R. Ravishankara, Chemical kinetics and photochemical data for use in stratospheric modeling, *JPL Publ., 90-1*, 17-91, 1990.

Fleming, E. L., S. Chandra, J. J. Burnett, and M. Corney, Zonal mean temperature, pressure, zonal winds and geopotential height as functions of latitude, *Adv. Space Res., 10*(12), 11-59, 1990.

Gardner, C. S., and D. G. Voelz, Lidar studies of the nighttime sodium layer over Urbana, Illinois, 2. Gravity waves, *J. Geophys. Res., 92*, 4673-4694, 1987.

Granier, C., J. P. Jegou, M. L. Chanin, and G. Megie, General theory of the alkali metals present in the Earth's upper atmosphere, III, Diurnal variations, *Ann. Geophys., 3*(4), 445-450, 1985.

Hedin, A. E., Thermospheric model, *J. Geophys. Res., 92*, 4649, 1987.

Helmer, M., and J. M. C. Plane, A study of the reaction $NaO_2 + O \rightarrow NaO + O_2$, implications for the chemistry of sodium in the upper atmosphere, *J. Geophys. Res., 98*, 23207-23222, 1993.

Herschbach, D. R., C. E. Kolb, D. R. Worsnop and X. Shi, Excitation mechanism of the mesospheric sodium nightglow, *Nature, 356*, 414-416, 1992.

Hocking W. K. COSPAR International Reference Atmosphere: 1986, Part II: Middle atmosphere models, *Adv. Space Res., 10*(10), 153-161, 1990.

Hunten, D. M., Spectroscopic studies of the twilight airglow, *Space Sci. Reviews, 6*, 493-573, 1967.

Hunten, D. M., A meteor-ablation model of the sodium and potassium layers, *Geophys. Res. Lett., 8*, 369-372, 1981.

Hunten, D. M., R. P. Turco, and O. B. Toon, Smoke and dust particles of meteoric origin in the mesosphere and stratosphere, *J. Atmos. Sci., 37*, 1342-1357, 1980.

Jegou, J. P., C. Granier, M. L. Chanin, and G. Megie, General theory of the alkali metals present in the Earth's upper atmosphere, I, Flux model: Chemical and dynamical processes, *Ann. Geophys., 3*, 163-176, 1985a.

Jegou, J. P., C. Granier, M. L. Chanin, and G. Megie General theory of the alkali metals present in the Earth's upper atmosphere, II, Seasonal and meridional variations, *Ann. Geophys., 3*(3) 299-312, 1985b.

Junge, C. E., O. Oldenberg, and J. T. Wasson, On the origin of the sodium present in the upper atmosphere, *J. Geophys. Res., 67*, 1027-1039, 1962.

Keating, G. M., M. C. Pitts, and D. F. Young, COSPAR International Reference Atmosphere: 1986, Part II: Middle atmosphere models, *Adv. Space Res., 10(12)*, 317-355, 1990.

Kirchhoff, V. W. J. H., Atmospheric sodium chemistry and diurnal variations: An up-date, *Geophys. Res. Lett., 10*, 721- 724, 1983.

Kirchhoff, V. W. J. H., B. R. Clemesha, and D. M. Simonich, the atmospheric neutral sodium layer, I, Recent modeling compared to measurements, *J. Geophys. Res., 66*, 6892-6898, 1981.

Lin, C. L., and M. T. Leu, Temperature and third body dependence of the rate constant for the reaction $O + O_2 \rightarrow O_3 + M$, *Int. J. Chem. Kinetics, 14*, 417, 1982.

Lopez-Gonzalez, M. J., J. J. Lopez-Moreno, and R. Rodrigo, The altitude profile of the infrared atmospheric system of O_2 in twilight and early night: Derivation of ozone abundances, *Planet Space Sci., 40*, 1391-1397, 1992.

McDade, I. C., and E. J. Llewellyn, Kinetic parameters related to sources and sinks of vibrationally excited OH in the nightglow, *J. Geophys. Res., 92*, 7643-7650, 1987.

McDade, I. C., D. P. Murtagh, R. G. H. Greer, P. H. G. Dickinson, G. Witt, J. Stegman, E. J. Llewellyn, L. Thomas, and D. B. Jenkins, ETON 2: Quenching parameters for the proposed precursors of $O_2(b^1\Sigma_g^+)$ and $O(^1S)$ 557.7 nm in the terrestrial nightglow, *Planet. Space Sci., 34*, 789, 1986.

Megie, G., and J. E. Blamont, Laser sounding of atmospheric sodium interpretation in terms of global atmospheric parameters, *Planet. Space Sci., 25*, 1093-1109, 1977.

Murad, E., and W. Swider, Chemistry of meteor metals in the stratosphere, *Geophys. Res. Lett., 6*, 929-932, 1979.

Murphy, R. E., Infrared emission of OH in the fundamental and first overtone bands, *J. Chem. Phys., 54*, 4852-4859, 1971.

Murtagh, D. P., R. G. H. Greer, I. C. McDade, E. J. Llewellyn, and M. Bantle, representative volume emission profiles from rocket photometer data, *Ann. Geophys., 2*, 467-474, 1984.

Murtagh, D. P., G. Witt, J. Stegman, I. C. McDade, E. J. Llewellyn, F. Harris, and R. G. H. Greer, An assessment of proposed $O(^1S)$ and $O_2(b^1\Sigma_g^+)$ nightglow excitation parameters, *Planet. Space Sci., 38*, 43-53, 1990.

Plane, J. M. C., The chemistry of meteoric metals in the Earth's upper atmosphere, *Int. Rev. Phys. Chem., 10*, 55-106, 1991.

Plane, J. M. C., and D. Husain, Determination of the absolute rate constant for the reaction $O + NaO \rightarrow Na + O_2$ by time-resolved atomic chemiluminescence at $\lambda = 589$ nm ($Na(3^2P_1) \rightarrow Na(3^2S_{1/2}) + h\nu$), *J. Chem. Soc. Faraday Trans. 2*, 82, 2047-2052, 1986.

Plane, J. M. C., C. -F. Nien, M. R. Allen, and M. Helmer, A kinetic investigation of the reactions $Na + O_3$ and $NaO + O_3$ over the temperature range 207-377 K, *J. Phys. Chem., 97*, 4459- 4467, 1993.

Rajasekhar, B., and J. M. C. Plane, An ab initio study of dissociative electron attachment to $NaHCO_3$ and $NaCO_3$, and the role of these reactions in the formation of sudden sodium layers, *Geophys. Res. Lett., 20*, 21-24, 1993.

Richter, E. S., and J. C. F. Sechrist, A meteor ablation-cluster ion atmospheric sodium theory, *Geophys. Res. Lett., 6*, 183-186, 1979.

Sharp, W. E., and D. Kita, In situ measurement of atomic hydrogen in the upper mesosphere, *J. Geophys. Res., 92*, 4319- 4325, 1987.

Shi, X., D. R. Herschbach, D. R. Worsnop, and C. E. Kolb, Molecular beam chemistry: magnetic deflection analysis of monoxide electronic states from the alkali-metal atom + ozone reactions, *J. Phys. Chem., 97*, 2113-2122, 1993.

Simonich, D. M., B. R. Clemesha, and V. W. J. H. Kirchhoff, The mesospheric sodium layer at 23°S: Nocturnal and seasonal variations, *J. Geophys. Res., 84*, 1543-1550, 1979.

Solomon, S., J. T. Kiehl, B. J. Kerridge, E. E. Remsberg, and J. M. Russell III, Evidence for nonlocal thermodynamic equilibrium in the v3 mode of mesospheric ozone, *J. Geophys. Res., 91*, 9865-9876, 1986.

Swider, W., Mesospheric sodium: Implications using a steady-state model, *Planet. Space Sci., 34*, 603-608, 1986.

Sze, N. D., M. K. W. Ko, W. Swider, and E. Murad, Atmospheric sodium chemistry I. The altitude region 70-100 km, *Geophys. Res. Lett., 9*, 1187-1190, 1982.

Takahashi, H., B. R. Clemesha, Y. Sahai, P. P. Batista, A. Eras, A. H. P. Chaves, B. Rosire, and J. R. Daniel, Rocket observations of the atomic and molecular oxygen emissions in the equatorial region, *Adv. Space Res., 10(10)*, 47-50, 1987.

Thomas, L., M. C. Isherwood, and M. R. Bowman, A theoretical study of the height distribution of sodium in the mesosphere, *J. Atmos. Terr. Phys., 45*, 587-594, 1983.

Tilgner, C., and U. von Zahn, Average properties of the sodium density distribution as observed at 69°N latitude in winter, *J. Geophys. Res., 93*, 8439-8454, 1988.

Worsnop, D. R., M. S. Zahniser, and C. E. Kolb, Low temperature absolute rate constants for the reaction of atomic sodium with ozone and nitrous oxide, *J. Phys. Chem., 95*, 3960-3964, 1991.

Wright, T. G., A. M. Ellis, and J. M. Dyke, A study of the products of the gas-phase reactions $M + N_2O$ and $M + O_3$, where M = Na or K, with ultraviolet photoelectron-spectroscopy, *J. Chem. Phys., 98*, 2891-2907, 1993.

B. R. Clemesha, S. M. L. Melo, D. M. Simonich, and H. Takahashi, INPE, C.P. 515, S.J. dos Campos, SP 12201-970, Brazil. (e-mail: inpedaa@eu.ansp.br)

J. M. C. Plane, School of Environmental Sciences, University of East Anglia, Norwich NR4 7TJ, England. (e-mail: J.Plane@east-anglia.ac.uk)

(Received August 24, 1994; revised March 28, 1995;
accepted March 28, 1995.)

Id: 7168
Au: Clemesha, Barcly Robert; Simonich, Dale Martin; takahashi, Hisao; Melo, H.; Plane, S.M.L..
Ti: Experimental evidence for photochemical control of the atmospheric sodium layer.
Fo: Journal of Geophysical Research; 100(:):18909-18916,
Lo: INPE-5752-PRE/1913.